Research Article

Dynamic Modelling and Continuous Trajectory Tracking Control of Space Robots Based on Lie Group SE(3)

Yong Wang [ID],[1] Kejie Gong,[2] Yurui Duan,[2] Boyong He,[1] and Hong Ma[1]

[1]*State Key Laboratory of Astronautic Dynamics, Xi'an 710043, China*
[2]*Key Laboratory for Fault Diagnosis and Maintenance of Spacecraft in-Orbit, Xi'an 710043, China*

Correspondence should be addressed to Yong Wang; wangyong08@nudt.edu.cn

For space robots, it is difficult to track continuous time-varying manifolds on SE(3) by using traditional closed-loop control strategies, which are designed to track the position and the attitude separately. Therefore, the dynamics model should be rebuilt, and the corresponding control strategy should be redesigned. Firstly, the dynamics equations for a space robot in the joint space and workspace are established separately in the framework of Lie group SE(3) and screw theory based on the Lagrange principle. Secondly, based on the proposed feedback form, a PD (proportional derivative) control law of output force on the end-effector is designed, and a closed-loop continuous tracking control strategy is proposed using the force Jacobian matrix and the kinematic model. The simulation results show that the control scheme has good performance when the system state changes gently. Furthermore, a robust sliding mode tracking control scheme is designed. The simulation results show that the proposed robust control law has better accuracy than the PD control law because the system state changes wildly. Finally, a robust fuzzy sliding mode tracking control scheme is designed to deal with the chattering phenomenon. The simulation results show that the proposed robust fuzzy control law can eliminate the chattering well and decrease the joint control torque significantly. The robustness of the proposed robust fuzzy control law is also verified by numerical simulation.

1. Introduction

The emergence of on-orbit assembly stems from the growing need to build large space structures [1]. Related technology has been greatly promoted through the development of on-orbit service technology, especially the on-orbit demonstration of space robot technology. However, the process of assembling large space structures is so elaborate that it requires an accurate and reliable operation ability for space robots. Accordingly, a proper motion planning method and corresponding tracking control strategy should be introduced. Due to the advantages beyond traditional theory, Lie group SE(3) and screw theory have been applied to research in space robotics, such as kinematic modelling [2] and trajectory planning. However, compatible dynamics and tracking control strategy are not considered in detail.

The dynamics of space robots belong to the category of multibody system dynamics. Thus, the modelling is mainly based on the Newton-Euler method and the Lagrange method. The former analyzes the forces of each rigid body based on classical Newtonian mechanics and then obtains dynamic equations in iterative form according to the relationship of internal forces [3]. The advantages of such a method are the clear physical meaning and the relatively small calculation [4]. However, the equations will become more complicated as the number of rigid bodies increases [5]. The Lagrange method is based on the Hamiltonian principle, and the dynamic relationship between the system state variables and the generalized forces is built based on the conservation of energy [6]. The advantages of such a method are that modelling process is relatively easy, and the dynamic equation is in the analytic form [7], but the physical meaning is not clear, and the partial differential calculation is more complex. A detailed comparison of these two methods is presented in [8].

In addition, the Kane method is also introduced in robotic dynamics research [9]. This method subtly uses the partial velocity as the generalized coordinate, which is

combined with the concept of generalized force to establish the dynamic equations according to the Darenbel-Lagrange principle [10]. The Kane method combines the advantages of the Newton-Euler and Lagrange methods, which have high calculation efficiency and concise form. Some improvement methods are proposed [11, 12], which further enhance the performance of the Kane method. Xu and Huang [13] compare classical methods with the Kane method and deduce the dynamic equations of a five-DOF robot using both methods. Yin and Ge [14] derive the dynamic equations of a dual-arm space robot using the Kane-Huston method and verify the feasibility with simple simulation.

Traditional dynamics modelling, which is based on geometric relationships, makes the derivation process relatively complicated. It brings a lot of convenience by introducing the Lie group and Lie algebra, which have a concise and unified form and decreases the difficulty of theoretical derivation. The theory of the Lie group has been applied to the dynamics of fixed-base robots [15, 16]. Besides, Liu et al. [17] combine the screw theory and the Kane method and propose a new concept of space robot dynamics.

Trajectory tracking control is crucial to accomplishing the task for the space robots, and the performance of the tracking controller determines the accuracy and reliability of the task. Many trajectory-tracking control strategies are designed based on the dynamic model. And some control theories for fixed-base ground robots can be introduced to tracking control of space robots, such as decomposition rate control [18], calculating torque control [19], robustness control [20], and reinforcement learning control [21]. Traditional dynamics modelling, which is based on geometric relationships, makes the derivation process relatively complicated.

Trajectory tracking of space robots can be performed either in joint space or in cartesian space. According to tracking targets, it can be further classified into point-to-point and continuous trajectory tracking. The latter means that the end-effector is required to move along the desired continuous trajectory, such as peg-in-hole insertion [22], which makes tracking control relatively difficult. Li and Liang [23] establish the kinematic equation of the space robot system by using the D-H (Denavit-Hartenberg) method and design the continuous trajectory control algorithm according to the momentum conservation law. Such an algorithm could be extended to a space robot with an arbitrary tree structure. Galicki [24] defines a nonsingular terminal sliding model in the workspace and proposes a robustness controller based on the Jacobian transfer, which can effectively eliminate the uncertainty of dynamics. Su et al. [25] define an approximately fixed-time convergence terminal sliding model and design a nonsingular sliding model tracking control strategy, but it is carried out in the joint space. In addition, most existing trajectory tracking control laws use position or linear velocity as feedback variables. There are also attempts that use quaternion [26] or dual quaternion [27] as feedback variables, but they are all difficult to apply to the tracking of the continuous time-varying manifold on SE(3).

Above all, this paper will focus on the dynamics modelling under the framework on Lie group SE(3) and the con-

trol problem of tracking the continuous time-varying trajectory of the end-effector on SE(3). Highlights of this paper are addressed below.

(1) The dynamic model of a multiarm space robot is established by combining the Lie group SE(3) with the Lagrange method. The model has a concise and unified form, which can decrease the difficulty of theoretical derivation and calculation

(2) A novel form is proposed to describe the feedback error in the tracking control problem of the space robot. Lie group SE(3) and screw theory are used to build the form, which can assemble the position and attitude, with their derivative, of the end-effector in a unified variable. It can significantly reduce the calculation in the process of closed-loop control

(3) A robust fuzzy sliding mode tracking control strategy is proposed to track the continuous and time-varying trajectory, including position and attitude together, of the end-effector. The tracking control strategy has good control accuracy, good robustness, and no chatter

2. Dynamic Modelling

2.1. Dynamic Equations of the Space Robot System. For a dual-arm space robot, as provided in Figure 1, the kinetic energy of the link of the arm in the barycentre-fixed inertial coordinate system is

$$T_i^k = \frac{1}{2}\left[\left(\boldsymbol{\omega}_{ki}^B\right)^{\mathrm{T}} I_{C_i^k} \boldsymbol{\omega}_{ki}^B + m_i^k \left({}^I\dot{\boldsymbol{p}}_i^k\right)^{\mathrm{T}I}\dot{\boldsymbol{p}}_i^k\right]\left(i = 0, 1, \cdots, n^k; k = 1, 2\right),$$

(1)

where ω_{ki}^B, $I_{C_i^k}$, m_i^k, and ${}^I\dot{\mathrm{p}}_i^k$ are the body angular velocity, the inertia, the mass, and the velocity, respectively. $i = 0$ refers to the base.

According to the definition of body velocity in screw theory, formula (1) can be transformed into the following form:

$$
\begin{aligned}
T_i^k &= \frac{1}{2}\left[\left(\boldsymbol{\omega}_{ki}^B\right)^{\mathrm{T}} I_{C_i^k}\boldsymbol{\omega}_{ki}^B + m_i^k\left(\left({}^I R_i^k\right)^{\mathrm{T}I}\dot{\mathrm{p}}_i^k\right)^{\mathrm{T}}\left({}^I R_i^k\right)^{\mathrm{T}I}\dot{\mathrm{p}}_i^k\right] \\
&= \frac{1}{2}\begin{bmatrix}\boldsymbol{\omega}_{ki}^B \\ \left({}^I R_i^k\right)^{\mathrm{T}I}\dot{\mathrm{p}}_i^k\end{bmatrix}^{\mathrm{T}}\begin{bmatrix}I_{C_i^k} & \boldsymbol{0} \\ \boldsymbol{0} & m_i^k E\end{bmatrix}\begin{bmatrix}\boldsymbol{\omega}_{ki}^B \\ \left({}^I R_i^k\right)^{\mathrm{T}I}\dot{\mathrm{p}}_i^k\end{bmatrix} \\
&= \frac{1}{2}\left({}^I_{C_i^k}\boldsymbol{V}^B\right)^{\mathrm{T}}\begin{bmatrix}I_{C_i^k} & \boldsymbol{0} \\ \boldsymbol{0} & m_i^k E\end{bmatrix}{}^I_{C_i^k}\boldsymbol{V}^B,
\end{aligned}
$$

(2)

where ${}^I_{C_i^k}\boldsymbol{V}^B$ is the body velocity, and ${}^I R_i^k$ represents the attitude rotation matrix in the inertial coordinate system.
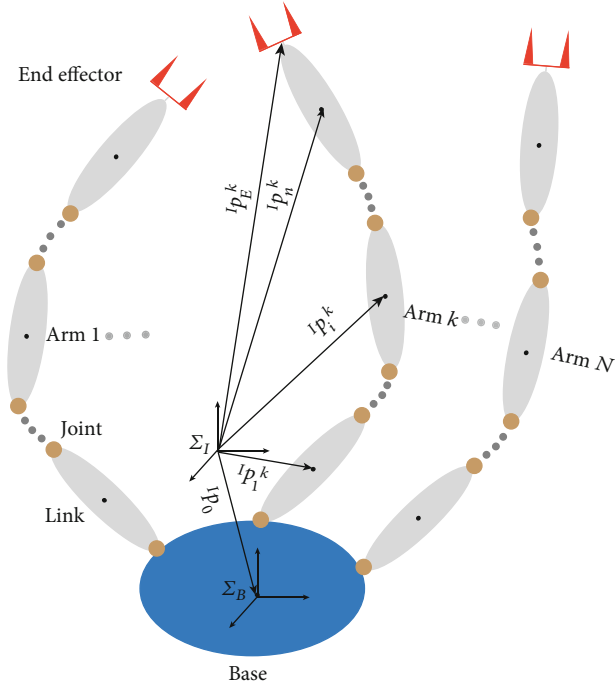
FIGURE 1: The model of a dual-arm space robot, which has two arms, and each arm has n^k joints.

According to the relationship between body velocity and spatial velocity, formula (2) is transformed into

$$
\begin{aligned}
T_i^k &= \frac{1}{2}\left(Ad_{(g_{ik})}{}_{C_i^k}^{I}\mathbf{V}^S\right)^{\mathrm{T}}\begin{bmatrix}\mathbf{I}_{C_i^k} & \mathbf{0}\\ \mathbf{0} & m_i^k E\end{bmatrix}Ad_{(g_{ik})}{}_{C_i^k}^{I}\mathbf{V}^S\\
&= \frac{1}{2}\left({}_{C_i^k}^{I}\mathbf{V}^S\right)^{\mathrm{T}}\left(Ad_{(g_{ik})}\right)^{\mathrm{T}}\begin{bmatrix}\mathbf{I}_{C_i^k} & \mathbf{0}\\ \mathbf{0} & m_i^k E\end{bmatrix}Ad_{(g_{ik})}{}_{C_i^k}^{I}\mathbf{V}^S\\
&= \frac{1}{2}\left({}_{C_i^k}^{I}\mathbf{V}^S\right)^{\mathrm{T}}\begin{bmatrix}{}^{I}R_i^k\mathbf{I}_{C_i^k}\left({}^{I}R_i^k\right)^{\mathrm{T}}-m_i^{kI}\widehat{\mathbf{p}}_i^{k}\,\widehat{\mathbf{p}}_i^{k} & m_i^{kI}\widehat{\mathbf{p}}_i^{k}\\ -m_i^{kI}\widehat{\mathbf{p}}_i^{k} & m_i^k E\end{bmatrix}{}_{C_i^k}^{I}\mathbf{V}^S\\
&= \frac{1}{2}\left({}_{C_i^k}^{I}\mathbf{V}^S\right)^{\mathrm{T}}K_i^{kI}{}_{C_i^k}\mathbf{V}^S,
\end{aligned}
\tag{3}
$$

where ${}_{C_i^k}^{I}\boldsymbol{V}^S$ is the spatial velocity, $Ad_{(g_{ik})}$ is the adjoint transformation, $\widehat{\cdot}$ represents the antisymmetric matrix of the corresponding vector, and $\boldsymbol{K}_i^k$ means generalized inertia matrix.

Therefore, the total kinetic energy of the dual-arm space robot is,

$$
\begin{aligned}
T &= \frac{1}{2}\left[\sum_{k=1}^{2}\sum_{i=1}^{n^k}\left({}_{C_i^k}^{I}\mathbf{V}^S\right)^{\mathrm{T}}\mathbf{K}_i^{kI}{}_{C_i^k}\mathbf{V}^S+\left({}_{B}^{I}\mathbf{V}^S\right)^{\mathrm{T}}\mathbf{K}_{0B}^{I}\mathbf{V}^S\right]\\
&= \frac{1}{2}\left[\sum_{k=1}^{n}\sum_{i=1}^{n^k}\left({}_{B}^{I}\mathbf{V}^S+Ad_{Bg}{}_{C_i^k}^{B}\mathbf{V}^S\right)^{\mathrm{T}}\mathbf{K}_i^k\left({}_{B}^{I}\mathbf{V}^S+Ad_{Bg}{}_{C_i^k}^{B}\mathbf{V}^S\right)\right)+\left({}_{B}^{I}\mathbf{V}^S\right)^{\mathrm{T}}\mathbf{K}_{0B}^{I}\mathbf{V}^S\right]\\
&= \frac{1}{2}\left[{}_{B}^{I}\mathbf{V}^S D+\sum_{k=1}^{n}\sum_{i=1}^{n^k}\left(Ad_{Bg}{}_{C_i^k}^{B}\mathbf{V}^S\right)^{\mathrm{T}}\mathbf{K}_i^k\left({}_{B}^{I}\mathbf{V}^S+Ad_{Bg}{}_{C_i^k}^{B}\mathbf{V}^S\right)\right],
\end{aligned}
\tag{4}
$$

where D represents the total momentum of the dual-arm space robot.

As is known, $D = 0$ is workable in the case of a free-floating base. Substituting GJM into formula (4) yields

$$
T = \frac{1}{2}\left[\sum_{k=1}^{2}\sum_{i=1}^{n^k}\left(Ad_{I_Bg}\boldsymbol{J}_i^k\dot{\boldsymbol{\theta}}\right)^{\mathrm{T}}\boldsymbol{K}_i^k\left(\boldsymbol{J}_B\dot{\boldsymbol{\theta}}+Ad_{I_Bg}\boldsymbol{J}_i^k\dot{\boldsymbol{\theta}}\right)\right]=\frac{1}{2}\dot{\boldsymbol{\theta}}^T\boldsymbol{H}\dot{\boldsymbol{\theta}},
\tag{5}
$$

where J_i^k are the GJM of the link and the base, respectively. $\dot{\boldsymbol{\theta}}$ is the angular velocity vector of all joints. $\boldsymbol{H}$ represents the generalized inertia tensor of the dual-arm space robot, the specific expression is as follows:

$$
\boldsymbol{H} = \sum_{k=1}^{2}\sum_{i=1}^{n^k}\left(Ad_{I_Bg}\boldsymbol{J}_i^k\right)^{\mathrm{T}}\boldsymbol{K}_i^k\left(\boldsymbol{J}_B+Ad_{I_Bg}\boldsymbol{J}_i^k\right)=\boldsymbol{J}_N^{\mathrm{T}}\tilde{\boldsymbol{K}}_{\mathrm{ver}}\boldsymbol{J}_B+\boldsymbol{J}_N^{\mathrm{T}}\tilde{\boldsymbol{K}}_{\mathrm{dia}}\boldsymbol{J}_N,
\tag{6}
$$

where

$$
\tilde{\boldsymbol{K}}_{\mathrm{ver}}=\begin{bmatrix}\boldsymbol{K}_1^1\\ \vdots\\ \boldsymbol{K}_{n^1}^1\\ \boldsymbol{K}_1^2\\ \vdots\\ \boldsymbol{K}_{n^2}^2\end{bmatrix}\in\mathbb{R}^{6n_d\times6},
$$

$$
\tilde{\boldsymbol{K}}_{\mathrm{dia}}=\begin{bmatrix}\boldsymbol{K}_1^1 & & & & &\\ & \ddots & & & &\\ & & \boldsymbol{K}_{n^1}^1 & & &\\ & & & \boldsymbol{K}_1^2 & &\\ & & & & \ddots &\\ & & & & & \boldsymbol{K}_{n^2}^2\end{bmatrix}\in\mathbb{R}^{6n_d\times6n_d}.
\tag{7}
$$

If the gravity is ignored and the joint elasticity is not considered, this system satisfies the Lagrange equation in the following form:

$$
\frac{\mathrm{d}}{\mathrm{d}t}\frac{\partial T}{\partial\dot{\boldsymbol{\theta}}}-\frac{\partial T}{\partial\boldsymbol{\theta}}=\boldsymbol{\tau}.
\tag{8}
$$

Substituting formula (5) into the above formula, then

$$
\boldsymbol{H}\ddot{\boldsymbol{\theta}}+\dot{\boldsymbol{H}}\dot{\boldsymbol{\theta}}-\frac{\partial}{\partial\boldsymbol{\theta}}\left(\frac{1}{2}\dot{\boldsymbol{\theta}}^{\mathrm{T}}\boldsymbol{H}\dot{\boldsymbol{\theta}}\right)=\boldsymbol{\tau}.
\tag{9}
$$

It can be rewritten as

$$H\ddot{\theta} + C\dot{\theta} = \tau, \tag{10}$$

where

$$C\dot{\theta} = \dot{H}\dot{\theta} - \frac{\partial}{\partial\theta}\left(\frac{1}{2}\dot{\theta}^{\mathrm{T}}H\dot{\theta}\right), \tag{11}$$

which represents the centrifugal force and Coriolis force.

For a single-arm space robot, the above derivation process is also applicable.

2.2. Static Force Jacobian Matrix. Static force Jacobian matrix is also a fundamental concept in the dynamics of space robots. Similar to the speed Jacobian matrix, it describes the mapping relationship between the output force on the end effector and the joint torque. This derivation is based on the equivalence principle of work and energy. Taking a single-arm space robot as an example, and assuming that the output force on the end effector is F^S, then the work is

$$W_\tau = \int_{t1}^{t2} \dot{\theta}^{\mathrm{T}}\tau\mathrm{d}t, \tag{12}$$

where $_E^I V^S$ is the spatial velocity of the end effector. Simultaneously, the work done by the joint torque τ is

$$W_\tau = \int_{t1}^{t2} \dot{\theta}^{\mathrm{T}}\tau\mathrm{d}t. \tag{13}$$

If joint friction is not considered, then W_F and W_τ should be equal and time-independent. Thus,

$$\left(_E^I V^S\right)^{\mathrm{T}} F^S = \dot{\theta}^{\mathrm{T}}\tau. \tag{14}$$

As is known, $V^S = J_E\dot{\theta}$, where J_E is the speed GJM of the end-effector for the joints. So

$$\tau = (J_E)^{\mathrm{T}} F^S, \tag{15}$$

where $(J_E)^{\mathrm{T}}$ is the static force Jacobian matrix.

2.3. Dynamic Equations in the Workspace. When performing trajectory tracking control of the end effector, it is also necessary to establish dynamic equations in the workspace. Firstly, according to the GJM of the end-effector, there are

$$\dot{\theta} = J_E^{-1}{}_E^I V^S, {}_E^I \dot{V}^S = J_E\ddot{\theta} + \dot{J}_E\dot{\theta}. \tag{16}$$

Accordingly,

$$\ddot{\theta} = J_E^{-1}\left(_E^I \dot{V}^S - \dot{J}_E J_E^{-1}{}_E^I V^S\right). \tag{17}$$

Substituting formula (17) into formula (10),

$$HJ_E^{-1}\left(_E^I \dot{V}^S - \dot{J}_E J_E^{-1}{}_E^I V^S\right) + CJ_E^{-1}{}_E^I V^S = \tau. \tag{18}$$

It can be rewritten as

$$HJ_E^{-1}{}_E^I \dot{V}^S + \left(C - HJ_E^{-1}\dot{J}_E\right)J_E^{-1}{}_E^I V^S = \tau. \tag{19}$$

Then, substituting formula (15) into the above formula,

$$H_g{}_E^I \dot{V}^S + C_g{}_E^I V^S = F^S, \tag{20}$$

where $H_g = (J_E)^{-\mathrm{T}}HJ_E^{-1}$ and $C_g = (J_E)^{-\mathrm{T}}(C - HJ_E^{-1}\dot{J}_E)J_E^{-1}$. It can be proved that the above dynamic equation satisfies,

(1) H_g is a symmetric positive definite matrix

(2) $\dot{H}_g - 2C_g$ is an antisymmetric matrix

2.4. Feedback Calculation Model Based on SE(3). As the desired trajectory is expressed on SE(3), compatible feedback should be designed first. Supposing that g_i and g_{di} are the actual and desired pose of the end effector, respectively, then the pose error can be written as

$$g_e = g_{di}^{-1} g_i, \tag{21}$$

where $g_e \in \mathrm{SE}(3)$.

The tracking error in exponential coordinate is presented as

$$\widehat{\xi}_e = \log_g\left(g_{di}^{-1} g_i\right), \tag{22}$$

where $\log_g(\cdot)$ represents the logarithmic mapping from Lie group SE(3) to its Lie algebra se(3).

The above equation can be written in the form of screw coordinates as

$$\xi_e^B = \left(\log_g\left(g_{di}^{-1} g_i\right)\right)^\vee. \tag{23}$$

It is used as feedback at the position level. It should be noted that ξ_e^B is with respect to the body-fixed coordinate system of the end effector.

The feedback at the velocity level can be expressed as

$$V_e^B = V_i^B - V_{di}^B, \tag{24}$$

where $V_i^B = \left(g_i^{-1}\dot{g}_i\right)^\vee$ is the actual body velocity, and $V_{di}^B = \left(g_{di}^{-1}\dot{g}_{di}\right)^\vee$ is the desired body velocity.

In fact, the following relationship exists:
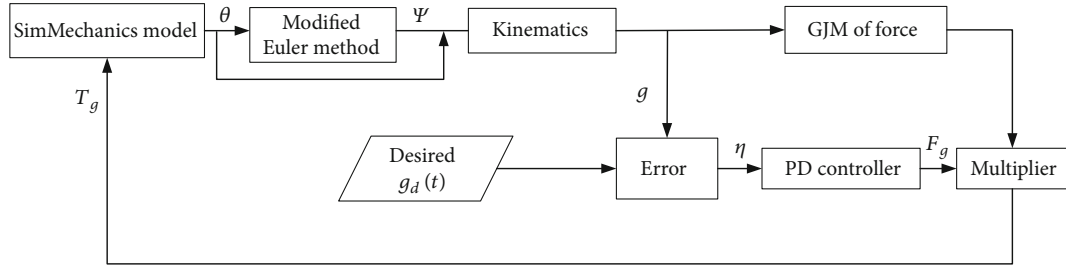
$$\dot{\xi} = G(\xi)V^B. \tag{25}$$

FIGURE 2: PD control block diagram based on the Jacobi matrix.

The expression of $G(\xi)$ in the above formula is presented in [28] and omitted here.

Accordingly, the feedback of pose expressed on SE(3) can be expressed as

$$\boldsymbol{\eta}^B = \begin{bmatrix} \boldsymbol{\xi}_e^B & \boldsymbol{V}_e^B \end{bmatrix}. \tag{26}$$

Transforming it into inertial coordinate system yields

$$\boldsymbol{\eta} = Ad_{g_i}\boldsymbol{\eta}^B = \begin{bmatrix} \boldsymbol{\xi}_e & \boldsymbol{V}_e \end{bmatrix}. \tag{27}$$

3. Continuous Trajectory Tracking Control Strategy

3.1. PD Controller Based on Jacobian Matrix.
According to the feedback $\boldsymbol{\eta}$ obtained in the previous section, the following PD control law is designed:

$$\boldsymbol{F}_g^{\mathcal{S}} = -\boldsymbol{K}_p\boldsymbol{\xi}_e - \boldsymbol{K}_v\boldsymbol{V}_e, \tag{28}$$

where $\boldsymbol{F}_g^{\mathcal{S}}$ is the output force on the end effector with respect to the inertial coordinate system, and $\boldsymbol{K}_p$ and $\boldsymbol{K}_v$ are the position and velocity gains, respectively.

Then, the joint control torque can be computed as

$$\boldsymbol{\tau}_g = (\boldsymbol{J}_E)^{\mathrm{T}}\mathbf{F}_g^{\mathcal{S}}. \tag{29}$$

Accordingly, detailed steps of a closed-loop tracking control strategy are given as follows (as shown in Figure 2):

Step 1. Set the initial joint angle $\boldsymbol{\theta}_0$ of the arm and the attitude $\boldsymbol{\Psi}_0$ of the base. Set the desired pose $g(t)$

Step 2. Calculate the current pose of the end effector according to the kinematics equation, and then obtain the force Jacobian matrix

Step 3. Calculate the current state feedback $\boldsymbol{\eta}$ according to formula (27)

Step 4. Calculate the joint control torque at the current moment according to formula (29)

Step 5. Calculate the joint angle $\boldsymbol{\theta}_i$ and joint angle rate $\dot{\boldsymbol{\theta}}_i$ at the next moment according to the dynamic equation, and then calculate the base attitude angle $\boldsymbol{\Psi}_i$ at the next moment

Step 6. Repeat steps 2-5 till to the end time.

The controllers proposed in this research include the PD controller, the robust sliding mode controller (RSMC), and the robust fuzzy sliding mode controller (RFSMC). RSMC or RFSMC can replace the PD controller module in Figure 2, and then the corresponding control block diagram is generated.

3.2. Robust Sliding Mode Tracking Controller.
The PD control has a simple form and can meet general needs. However, the control accuracy will be significantly reduced when the state changes fast. Considering the advantages of sliding mode control, such as the high control accuracy and strong robustness against external disturbances, a controller based on robust sliding mode control theory with the feedback calculation model above is proposed in this section.

3.2.1. Linear Reaching Law-Based Sliding Mode Control Law.
According to the tracking feedback at the velocity level, the sliding mode surface is designed as follows:

$$\boldsymbol{s} = \boldsymbol{V}_e + \Lambda\boldsymbol{\xi}_e = \boldsymbol{V} - \boldsymbol{V}_d + \Lambda\boldsymbol{\xi}_e, \tag{30}$$

where Λ is a positive definite diagonal matrix. A control law can be given

$$\boldsymbol{F}_g = \boldsymbol{H}_g(\boldsymbol{V}_d - \Lambda\boldsymbol{\xi}_e) + \boldsymbol{C}_g(\boldsymbol{V}_d - \Lambda\boldsymbol{\xi}_e) - \boldsymbol{K}_v\boldsymbol{s}, \tag{31}$$

where $\boldsymbol{K}_v$ is a positive definite diagonal matrix.

Theorem 1. *For the dynamics of a space robot system, applying sliding mode surface (30) and control law (31), the system will gradually converge to the equilibrium point.*

Proof. Define the Lyapunov function as follows:

$$L = \frac{1}{2}\boldsymbol{s}^{\mathrm{T}}\boldsymbol{H}_g\boldsymbol{s}. \tag{32}$$

According to the sliding mode surface (30),

$$\boldsymbol{V} = \boldsymbol{s} + \boldsymbol{V}_d - \Lambda\boldsymbol{\xi}. \tag{33}$$
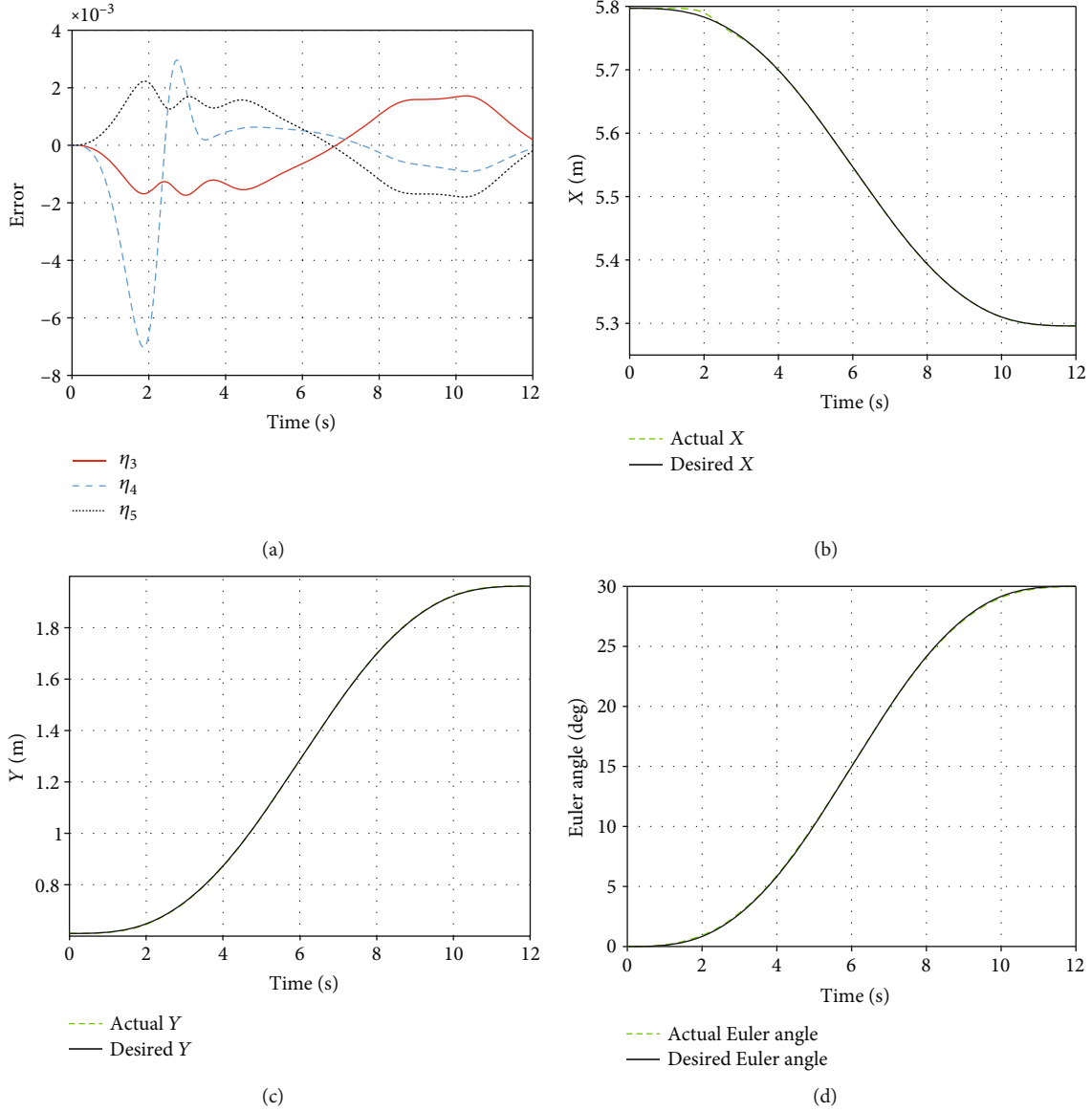
(a)

(b)

(c)

(d)

FIGURE 3: Error and pose components in the tracking process.

Calculating the derivation of L and substituting (28) into it yields

$$
\begin{aligned}
\dot{L} &= \mathbf{s}^{\mathrm{T}} \mathbf{H}_g \dot{\mathbf{s}} + \frac{1}{2} \mathbf{s}^{\mathrm{T}} \dot{\mathbf{H}}_g \mathbf{s} = \mathbf{s}^{\mathrm{T}} \mathbf{H}_g \left(\dot{\mathbf{V}}_d - \dot{\mathbf{V}}_e + \boldsymbol{\Lambda} \dot{\boldsymbol{\xi}}_e \right) + \frac{1}{2} \mathbf{s}^{\mathrm{T}} \dot{\mathbf{H}}_g \mathbf{s} \\
&= \mathbf{s}^{\mathrm{T}} \left(-\mathbf{H}_g \left(\dot{\mathbf{V}}_d - \boldsymbol{\Lambda} \dot{\boldsymbol{\xi}}_e \right) + \mathbf{H}_g \dot{\mathbf{V}} \right) + \frac{1}{2} \mathbf{s}^{\mathrm{T}} \dot{\mathbf{H}}_g \mathbf{s} \\
&= \mathbf{s}^{\mathrm{T}} \left(-\mathbf{H}_g \left(\dot{\mathbf{V}}_d - \boldsymbol{\Lambda} \dot{\boldsymbol{\xi}}_e \right) - \mathbf{C}_g \mathbf{V} + \mathbf{F}_g^S \right) + \frac{1}{2} \mathbf{s}^{\mathrm{T}} \dot{\mathbf{H}}_g \mathbf{s} \\
&= \mathbf{s}^{\mathrm{T}} \left(-\mathbf{H}_g \left(\dot{\mathbf{V}}_d - \boldsymbol{\Lambda} \dot{\boldsymbol{\xi}}_e \right) - \mathbf{C}_g (\mathbf{V}_d - \boldsymbol{\Lambda} \boldsymbol{\xi}_e) - \mathbf{C}_g \mathbf{s} + \mathbf{F}_g^S \right) \\
&\quad + \frac{1}{2} \mathbf{s}^{\mathrm{T}} \dot{\mathbf{H}}_g \mathbf{s} = \mathbf{s}^{\mathrm{T}} \left(-\mathbf{H}_g \left(\dot{\mathbf{V}}_d - \boldsymbol{\Lambda} \dot{\boldsymbol{\xi}}_e \right) - \mathbf{C}_g (\mathbf{V}_d - \boldsymbol{\Lambda} \boldsymbol{\xi}_e) + \mathbf{F}_g^S \right) \\
&\quad + \frac{1}{2} \mathbf{s}^{\mathrm{T}} \left(\dot{\mathbf{H}}_g - 2\mathbf{C}_g \right) \mathbf{s} = -\mathbf{s}^{\mathrm{T}} \mathbf{K}_v \mathbf{s} \leqslant -\lambda L,
\end{aligned}
$$

$$(34)$$

where $\lambda = \lambda_{\min}(K_v)/\lambda_{\max}(H_g)$. $\lambda_{\min}(K_v)$ is the smallest eigenvalue of $\mathbf{K}_v$, and $\lambda_{\max}(H_g)$ is the largest eigenvalue of $\mathbf{H}_g$. It can be seen that the sliding mode surface $\mathbf{s}$ converges to zero driven by the control law (31). If $\mathbf{s} \equiv 0$, there is $\mathbf{V}_e = -\boldsymbol{\Lambda}\boldsymbol{\xi}_e$, then $\boldsymbol{\xi}_e, \mathbf{V}_e$ progressively converge to the equilibrium point. Proof completed. □

3.2.2. Robust Sliding Mode Control Law. When the dynamic model can be accurately established, the sliding mode control law (31) can be substituted into the PD control strategy to replace the PD control law. However, as the dynamic model of the space robot is very complicated, if control law (31) is directly adopted not only will the modelling be complex but also the amount of calculation will be huge. Let

$$
\mathbf{f} = -\mathbf{H}_g (\mathbf{V}_d - \boldsymbol{\Lambda} \dot{\boldsymbol{\eta}}_e) - \mathbf{C}_g (\mathbf{V}_d - \boldsymbol{\Lambda} \boldsymbol{\eta}_e). \tag{35}
$$

Regard this term as a disturbance and assume that the term is bounded and satisfies the following inequality:

$$-H_g(V_d - \Lambda\dot{\eta}_e) - C_g(V_d - \Lambda\eta_e) \le D. \tag{36}$$

In order to overcome the disturbance term, the following sliding mode control law is designed:

$$F_g^S = -[K_v s + \rho \, \text{sgn}\,(s)], \tag{37}$$

where ρ is the robust coefficient and $\rho \le D$ and $\rho\,\text{sgn}\,(s)$ is the robust term to overcome the disturbance.

Theorem 2. *For the dynamics of a space robot system, applying sliding mode surface (30) and control law (37), the system will gradually converge to the equilibrium point.*

Proof. Define the Lyapunov function as follows:

$$L = \frac{1}{2}s^T H_g s. \tag{38}$$

Similar to Theorem (1),

$$
\begin{aligned}
\dot{L} &= s^T\left(-H_g\left(\dot{V}_d - \Lambda\dot{\xi}_e\right) - C_g(V_d - \Lambda\xi_e) + F_g^s\right) \\
&= s^T\left(-H_g\left(\dot{V}_d - \Lambda\dot{\xi}_e\right) - C_g(V_d - \Lambda\xi_e) - [K_v s + \rho\,\text{sgn}\,(s)]\right) \\
&\le -s^T K_v s + (D - \rho)\|s\| \le -\lambda L.
\end{aligned}
\tag{39}
$$

It can be proven like Theorem (1).
Proof completed. □

3.3. Robust Fuzzy Sliding Mode Tracking Controller considering Uncertainty. The robust sliding mode tracking controller has better control accuracy; however, when there are uncertainties with the parameters of the system model, the controller must choose a more significant robust coefficient or amplify the gain to ensure robust performance and control accuracy which may lead to the obvious chattering of the control torque. In order to solve this problem, fuzzy ideas are introduced into to sliding mode control law to approximate the dynamic model with uncertain parameters, which can realize robust and stable control of the space robot.

3.3.1. Fuzzy Approximation Method. Taking into account the unavoidable external interference, introduce the interference force F_g to the dynamic model as follow.

$$H_g\dot{V} + \tilde{C}_g\dot{V} = F_g + F_d. \tag{40}$$

The following fuzzy sliding mode control law is designed

$$F_g = -\hat{f} - K_v s, \tag{41}$$

where $\hat{f}$ is the estimated value of the fuzzy system. Substituting the control law into equation (40) to obtain

$$H_g\dot{s} = -Cs - \hat{f} - K_v s + f + F_d = -(C + K_v)s - \tilde{f} + F_d = -(C + K_v)s + \zeta_0, \tag{42}$$

where $\tilde{f} = \hat{f} - f$ and $\zeta_0 = -\tilde{f} + F_d$.

The fuzzy approximation can be used to estimate the function f in equation (35),

$$f = -H_g(V_d - \Lambda\dot{\eta}_e) - C_g(V_d - \Lambda\eta_e) = W^*\beta + \epsilon, \tag{43}$$

where W^* is the optimal weight matrix of the fuzzy approximation system, ϵ is the approximation error of the system, and β is the basis function.

Let $\hat{W}$ be the estimation of W^* and let the sliding mode surface s as the input variable of the basis function, and then the dynamic compensation part of the space robot control law is estimated to be

$$\hat{f} = \hat{W}\beta + \epsilon. \tag{44}$$

3.3.2. Robust Fuzzy Sliding Mode Tracking Control Law. Firstly, assuming that

(1) The output of the fuzzy approximation system is bounded, and the total external disturbance of the estimated system is bounded, which is expressed as

$$\|\hat{f}\| \le f_M. \tag{45}$$

(2) The estimation error of the fuzzy approximation system is bounded, which is expressed as

$$\|\epsilon\| \le \epsilon_M, \tag{46}$$

where ϵ_M is a positive constant.

(3) The estimated weight of the fuzzy approximation system is bounded, which is expressed as

$$tr\left(W^{*T}W^*\right) \le W_M, \tag{47}$$

where W_M is a positive constant.

The input variable of the fuzzy system is designed as

$$x = \left[s^T, \dot{s}^T\right]^T. \tag{48}$$

Then, the control law can be reshaped as

$$F_g = -\hat{W}\beta(x)K_v s - v, \tag{49}$$

where v is a robust term used to overcome approximation errors and interference. Let $\tilde{W} = \hat{W} - W^*$ be the estimation error of the optimal weight matrix.

According to the above control law, there is

$$
\begin{aligned}
H_g \dot{s} &= -(C + K_v)s - \hat{W}\beta - \epsilon + f + F_d - v \\
&= -(C + K_v)s - \tilde{W}\beta - \epsilon + F_d - v = -(C + K_v)s + \zeta_1,
\end{aligned}
\tag{50}
$$

where $\zeta_1 = -\tilde{W}\beta - \epsilon + F_d - v$, and $\|\epsilon\| \leq \epsilon_M$, $\|F_d\| \leq F_{dM}$.

The robust term v is designed as

$$
v = (\epsilon_M + F_{dM})sgn(s).
\tag{51}
$$

The adaptive updating law of the optimal weight matrix is taken as

$$
\dot{\hat{W}} = \sigma s \beta^T,
\tag{52}
$$

where σ is a positive constant.

Theorem 3. *For the dynamics of a space robot system considering interference, the fuzzy approximation method is used to estimate the uncertainty of the system, and the weight matrix updating law is set as formula (52), then the system under the action of the control law (49) will gradually converge to the equilibrium point.*

Proof. Define the Lyapunov function as follows:

$$
L_{fu} = \frac{1}{2}s^T H_g s + \frac{1}{2\sigma} tr\left(\tilde{W}^T \tilde{W}\right).
\tag{53}
$$

Derivation of the above formula is

$$
\dot{L}_{fu} = s^T H_g \dot{s} + \frac{1}{2}s^T \dot{H}_g s + \frac{1}{\sigma} tr\left(\tilde{W}^T \dot{\tilde{W}}\right).
\tag{54}
$$

Substituting equation (50) into the above equation,

$$
\begin{aligned}
\dot{L}_{fu} &= -s^T K_v \dot{s} + \frac{1}{2}s^T\left(\dot{H}_g - 2C_g\right)s + \frac{1}{\sigma} tr\left(\tilde{W}^T \dot{\tilde{W}}\right) \\
&\quad + s^T(-\epsilon + F_d - v) = -s^T K_v \dot{s} + \frac{1}{\sigma} tr\left(\tilde{W}^T \dot{\tilde{W}}\right) \\
&\quad + s^T\left(-\tilde{W}\beta\right) + s^T(-\epsilon + F_d - v) = -s^T K_v \dot{s} \\
&\quad + \frac{1}{\sigma} tr\left(\tilde{W}^T\left(\dot{\tilde{W}} - \sigma s \beta^T\right)\right) + s^T(-\epsilon + F_d - v).
\end{aligned}
\tag{55}
$$

Substituting the updating law (52) into the above equation,

$$
\dot{L}_{fu} = -s^T K_v \dot{s} + s^T(\epsilon + F_d - v),
\tag{56}
$$

due to

$$
\begin{aligned}
s^T(-\epsilon + F_d - v) &= s^T(-\epsilon + F_d) - s^T v \\
&= s^T(-\epsilon + F_d) - s^T(\epsilon_M + F_{dM}) \, \text{sgn}(s) \\
&= s^T(-\epsilon + F_d) - \|s\|(\epsilon_M + F_{dM}) \leq 0
\end{aligned}
\tag{57}
$$

Then, there is

$$
\dot{L}_{fu} \leq -s^T K_v \dot{s} \leq 0.
\tag{58}
$$

If $\dot{L}_{fu} \equiv 0$, then $s \equiv 0$. According to the LaSalle invariance principle, the closed-loop system has the property of gradual stability as $t \longrightarrow \infty$, $s \longrightarrow 0$. Thus, the error of the pose in exponential form and the velocity will gradually converge to zero as $\eta \longrightarrow 0$, $V_e \longrightarrow 0$; so the pose and velocity of the end-effector will gradually converge to desired values as $g \longrightarrow g_d$, $V \longrightarrow V_d$.

Proof completed.   □

4. Simulation Example

Considering a planar, three-DOF space robot as a simulation case and verifying the effectiveness and control performance of the proposed control strategies. The initial pose and the final pose are given as follows:

$$
\begin{aligned}
g_0 &= \begin{bmatrix} & & 5.797 \\ E_{3\times3} & & 0.6105 \\ & & 0 \\ 0 & & 1 \end{bmatrix}, \\
g_n &= \begin{bmatrix} & & 5.296 \\ R_z(30°) & & 1.9615 \\ & & 0 \\ 0 & & 1 \end{bmatrix}.
\end{aligned}
\tag{59}
$$

The desired trajectory $g_d(t)$ is planned based on the drive transformation method and screw theory.

4.1. Simulation Results of PD Controller. Simulations of the PD controller are performed in MATLAB/Simulink, and the results are obtained as follows. The state error varying with time is shown in Figure 3(a), as is seen in which the maximum error is about 8×10^{-3}, and the steady state error is less than 2×10^{-3}. Figures 3(b)–3(d) show the comparison between the actual and desired pose components. It can be seen that the tracking process is ideal.

The output force on the end effector and the joint control torque obtained by the PD control law is shown in Figures 4 and 5 separately. The joint control torque is relatively small, and no saturation occurs. The space robot's joint motions are shown in Figures 6 and 7. It can be seen
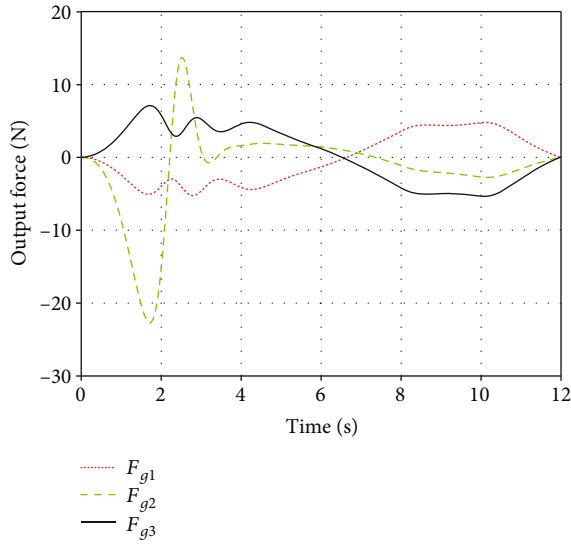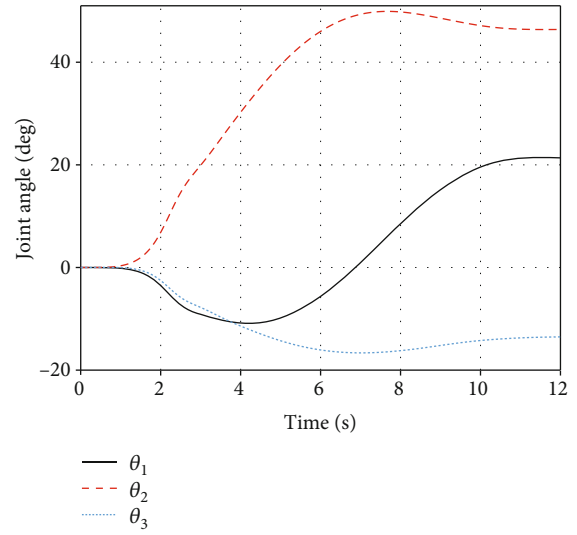
Figure 4: Output force.
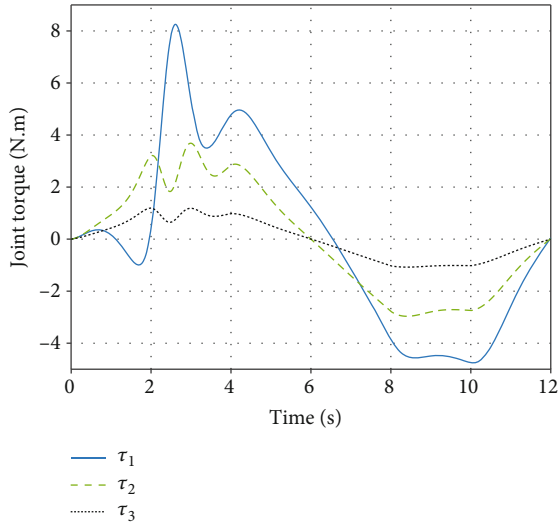

Figure 6: Joint angles.
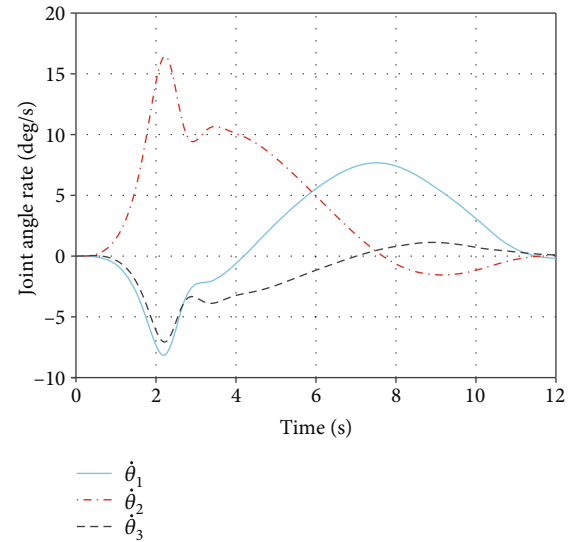

Figure 5: Joint control torque.

Figure 7: Angular velocity.

that the joint motions are continuous and smooth without sudden change. To sum up, the designed PD controller performs well under the gentle motion state.

4.2. Simulation Results of the Robust Sliding Mode Controller. The simulation object remains the same as in the previous section, and the initial and final poses remain unchanged. The desired trajectory is replanned to move faster. The parameters of the sliding mode controller are set as $K_v = \text{diag}\,([0, 0, 667, 667, 667, 0])$, $\Lambda = \text{diag}\,([0, 0, 4.20, 4.20, 4.20, 0])$, and $\rho = 3.3$.

The PD control strategy and the robust sliding mode tracking control strategy are simulated, respectively, and simulation results are obtained as follows. From comparisons of Figures 8(a) and 3(a), it can be seen that accuracy of PD control has been significantly reduced, the maximum

error has reached 0.013, and the steady-state error also increases. In the same situation, the accuracy of the robust sliding mode control is higher, the maximum error is about 9×10^{-3}, and the steady-state error remains within 2×10^{-3} as in Figure 8(b). Figures 9(a) and 9(b) show the joint control torque of the two control algorithms. In contrast, the control torque of sliding mode control has a specific chattering phenomenon.

4.3. Simulation Results of the Robust Fuzzy Sliding Mode Controller. The simulation object remains the same as in the previous section, and the initial and final poses remain unchanged. Set the parameters of the robust sliding mode controller as $K_v = \text{diag}\,([0, 0, 1067, 967, 967, 0])$, $\Lambda = \text{diag}\,([0, 0, 4.20, 4.20, 4.20, 0])$, and $\rho = 5$. Seven fuzzy
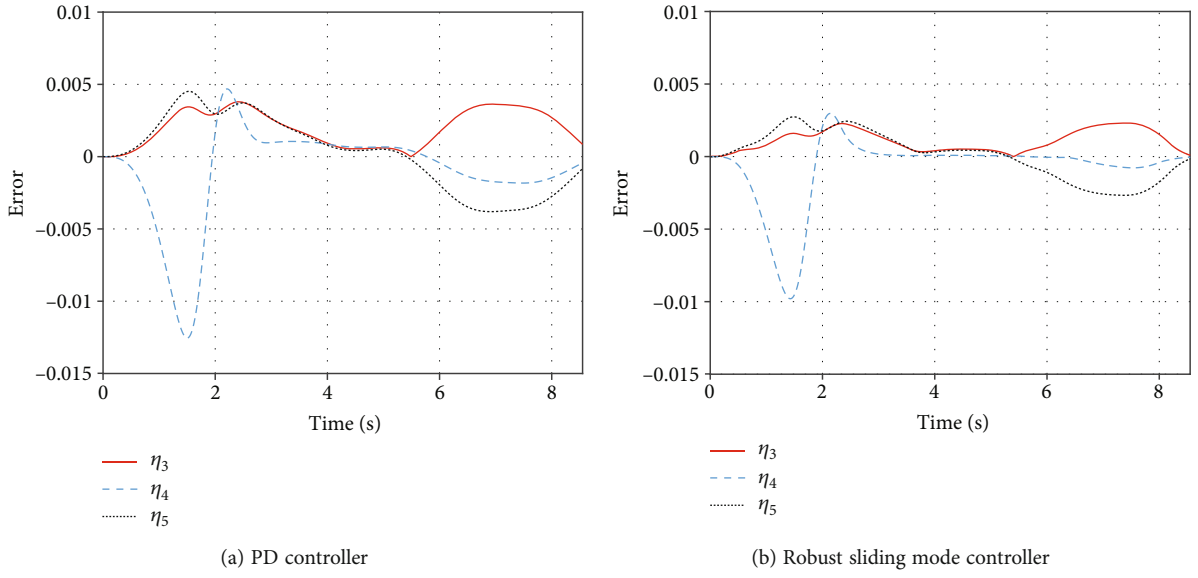
(a) PD controller

(b) Robust sliding mode controller

FIGURE 8: Comparison of tracking error of two control algorithms.

(a) PD controller
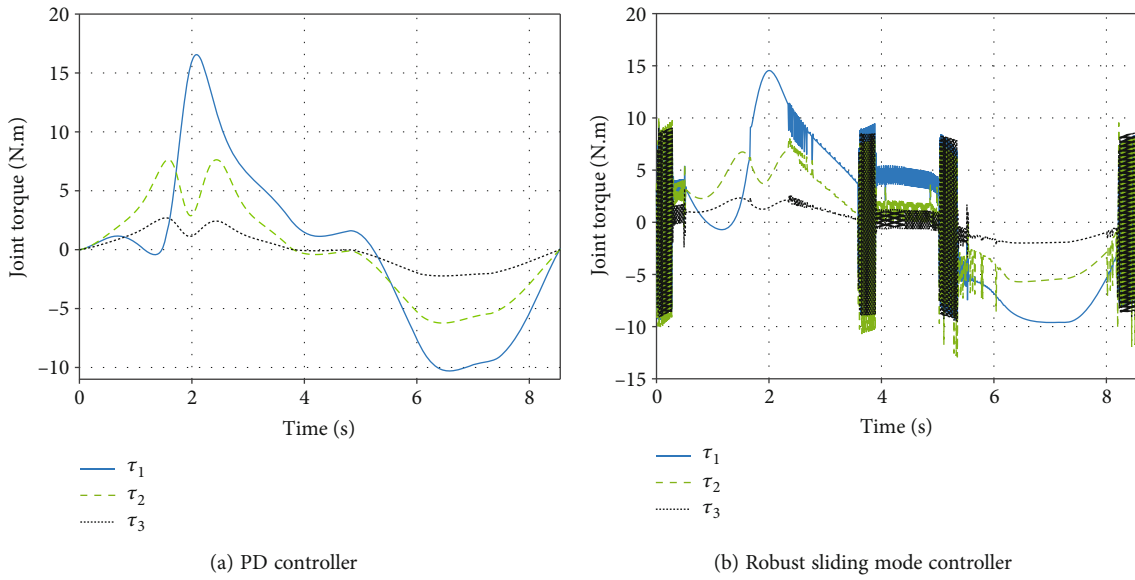
(b) Robust sliding mode controller

FIGURE 9: Comparison of joint control torque of the two control algorithms.

subjection functions of the fuzzy sliding mode controller are as follows:

$$\mu_{A_k^1}(x) = \frac{1}{1 + e^{5(x + (\pi/4))}},$$

$$\mu_{A_k^2}(x) = e^{-0.5\left(\frac{x+1}{0.25}\right)^2},$$

$$\mu_{A_k^3}(x) = e^{-0.5\left(\frac{x+0.5}{0.25}\right)^2},$$

$$\mu_{A_k^4}(x) = e^{-0.5\left(\frac{x}{0.25}\right)^2},$$

$$\mu_{A_k^5}(x) = e^{-0.5\left(\frac{x-0.5}{0.25}\right)^2},$$

$$\mu_{A_k^6}(x) = e^{-0.5\left(\frac{x-1}{0.25}\right)^2},$$

$$\mu_{A_k^7}(x) = \frac{1}{1 + e^{5(x - \pi/4)}}. \tag{60}$$

The robust sliding mode tracking control strategy and the robust fuzzy sliding mode tracking control strategy are simulated, respectively, and simulation results are obtained as follows. It can be seen in Figures 10(a) and 10(b) and
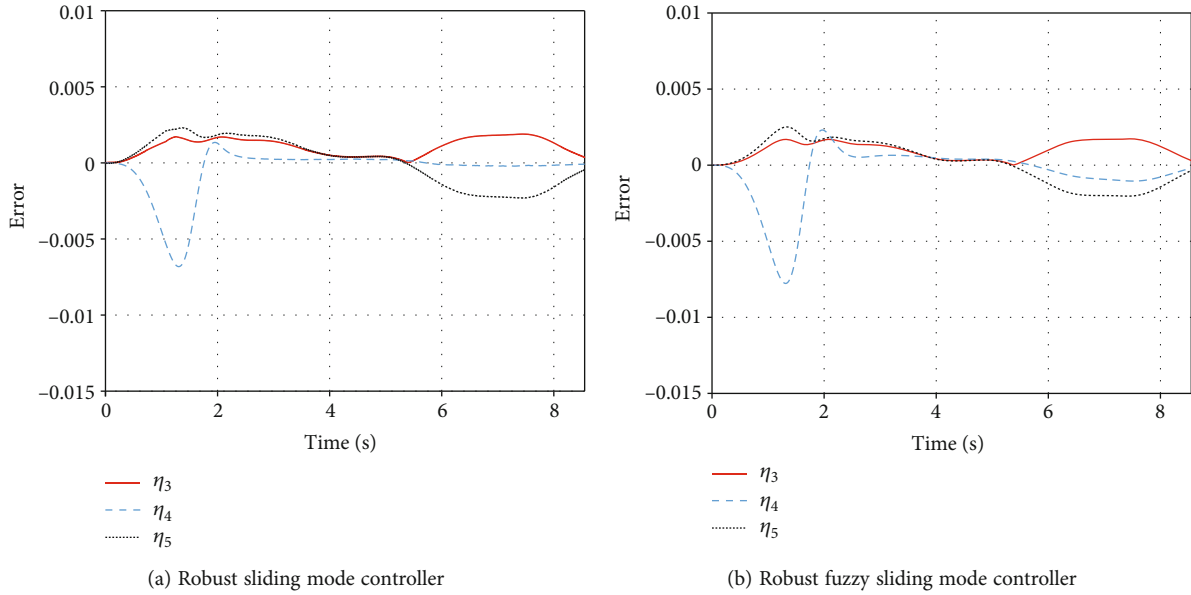
(a) Robust sliding mode controller

(b) Robust fuzzy sliding mode controller

FIGURE 10: Comparison of tracking error of two control algorithms.

(a) Robust sliding mode controller
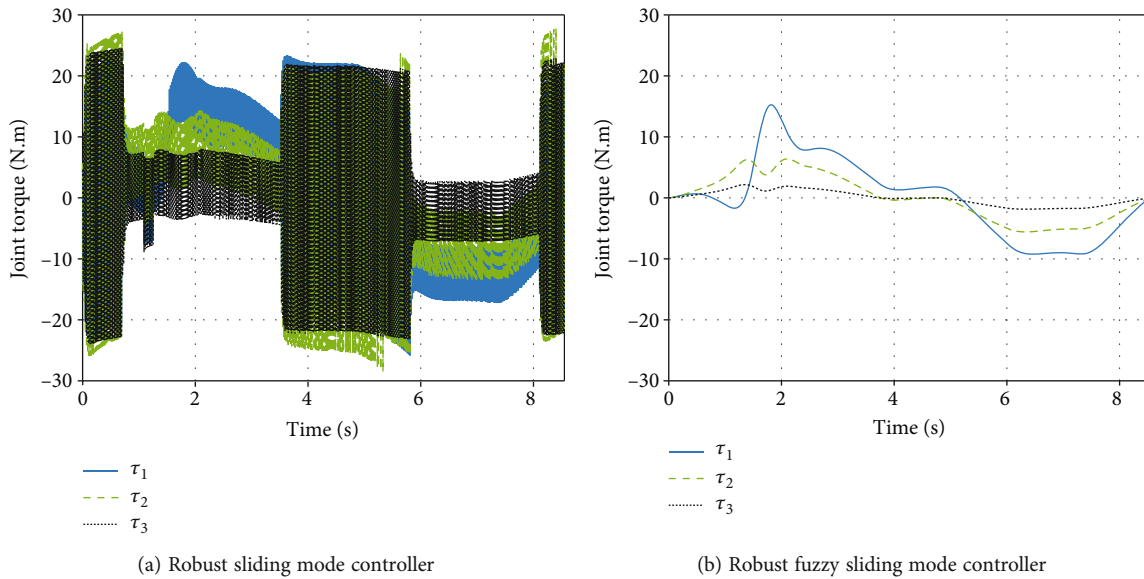
(b) Robust fuzzy sliding mode controller

FIGURE 11: Comparison of joint control torque of the two control algorithms.

Figures 11(a) and 11(b) that, after increasing the gain and robust coefficient of the robust sliding mode control, the control accuracy is improved. However, the joint control torque has serious chattering. In contrast, fuzzy sliding mode control can effectively eliminate chattering while ensuring similar accuracy, and the peak value of joint control torque is also significantly better. Figure 12 shows the output force of the end effector and the corresponding estimated value obtained during the fuzzy sliding-mode control algorithm process.

4.4. Simulation Results of Robust Fuzzy Sliding Mode Controller with Interference Force. In order to verify the robust performance of the fuzzy sliding mode controller, the interference force is set as follows:

$$
\boldsymbol{F}_d = \begin{bmatrix} 0 \\ 0 \\ 0.6 \sin\left(2t + \dfrac{\pi}{3}\right) \\ 0.5 \sin\left(3t + \dfrac{\pi}{4}\right) \\ 0.5 \sin\left(3t + \dfrac{\pi}{4}\right) \\ 0 \end{bmatrix}.
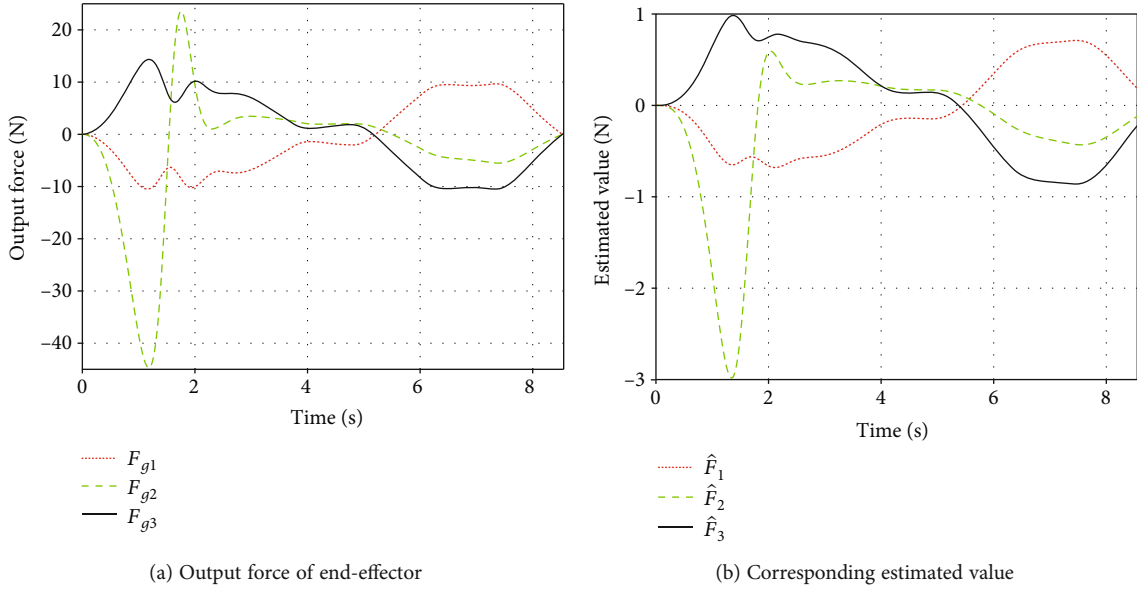\tag{61}
$$

(a) Output force of end-effector

(b) Corresponding estimated value

FIGURE 12: Output force of end-effector of robust fuzzy sliding mode controller.

(a) Tracking error
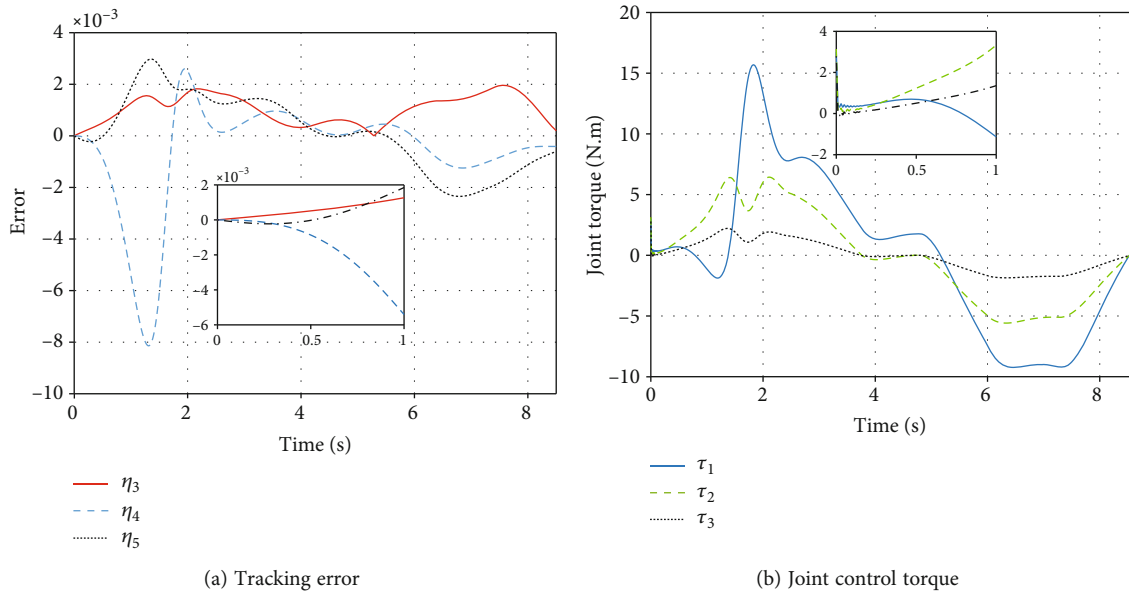

(b) Joint control torque

FIGURE 13: Simulation results of robust fuzzy sliding mode controller with interference force.

The simulation is performed under the same conditions as Section 4.3, and the following results are obtained. After the interference force is added, the state feedback error and joint control torque are shown in Figures 13(a) and 13(b). Comparing with Figures 10(b) and 11(b), respectively, it can be seen that the interference force only has an impact on the system within the first 1 s, which makes the error and joint torque amplify compared with when there is no disturbance, but keep it unanimous afterward. It demonstrates that the fuzzy sliding mode tracking controller has good robustness.

Furthermore, another simulation is performed with a pulse interference force set as follows:

$$F_{d1} = \begin{cases} \begin{bmatrix} 0 \\ 0 \\ -2 + 0.6 \sin\left(2t + \dfrac{\pi}{3}\right) \\ -2 + 0.5 \sin\left(3t + \dfrac{\pi}{4}\right) \\ -2 + 0.5 \sin\left(3t + \dfrac{\pi}{4}\right) \\ 0 \end{bmatrix}, & 3 < t < 5, \\ \\ F_d, & \text{other}. \end{cases} \tag{62}$$
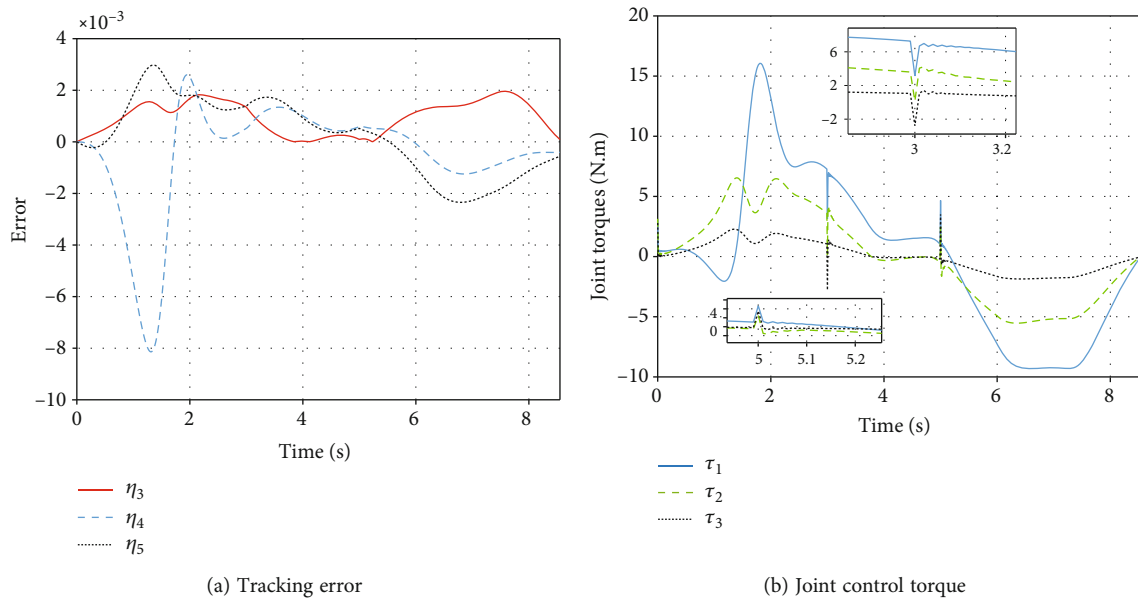
(a) Tracking error

(b) Joint control torque

FIGURE 14: Simulation results of robust fuzzy sliding mode controller with pulse interference force.

Following results are obtained. It can be seen in Figure 14(a) that the error keeps very similar, while the joint control torque fluctuates slightly in the third and fifth seconds in Figure 14(b); however, the system can still keep stable after the pulse, which demonstrates the robustness of the fuzzy sliding mode tracking controller again.

5. Conclusion

Firstly, based on the Lagrange principle and the generalized Jacobian matrix, the dynamic equations in the joint space and workspace are established separately. Then, a feedback calculation model is proposed based on the screw theory. Furthermore, the PD and robust fuzzy sliding mode control laws are designed separately. Finally, the closed-loop control strategies are constructed by integrating control laws, the GJM, a dynamic model, and a kinematic model. The effectiveness of each control law is verified by simulations, and the control accuracy and performance are compared and analyzed. It can be summarized that the proposed dynamic modelling method is feasible and efficient. The PD controller is proven to have relatively high control accuracy. Nevertheless, the accuracy reduces when the system state changes more dramatically. The robust sliding mode controller is able to overcome such disadvantages, and the fuzzy sliding mode controller could solve the chattering problem.

Data Availability

The data used to support the findings of this study are included within the article.

Conflicts of Interest

The authors declare that there is no conflict of interest regarding the publication of this paper.

References

[1] K. Cao, S. Li, Y. She, J. D. Biggs, Y. Liu, and L. Bian, "Dynamics and on-orbit assembly strategies for an orb-shaped solar array," *Acta Astronautica*, vol. 178, pp. 881–893, 2021.

[2] Y. Wang, X. Liang, K. Gong, and Y. Liao, "Kinematical research of free-floating space-robot system at position level based on screw theory," *International Journal of Aerospace Engineering*, vol. 2019, Article ID 6857106, 13 pages, 2019.

[3] A. Jain and G. Rodriguez, "Base-invariant symmetric dynamics of free-flying manipulators," *IEEE Transactions on Robotics and Automation*, vol. 11, no. 4, pp. 585–597, 1995.

[4] W. Xu, C. Li, X. Wang, Y. Liu, B. Liang, and Y. Xu, "Study on non-holonomic cartesian path planning of a free-floating space robotic system," *Advanced Robotics*, vol. 23, no. 1-2, pp. 113–143, 2009.

[5] R. Featherstone and D. Orin, "Robot dynamics: equations and algorithms," in *Proceedings 2000 ICRA. Millennium Conference. IEEE International Conference on Robotics and Automation. Symposia Proceedings (Cat. No.00CH37065)*, pp. 826–834, San Francisco, CA, USA, 2000.

[6] Y. Xu and H. Y. Shum, "Dynamic control and coupling of a free-flying space robot system," *Journal of Robotic Systems*, vol. 11, no. 7, pp. 573–589, 1994.

[7] P. J. From, V. Duindam, K. Y. Pettersen, J. T. Gravdahl, and S. Sastry, "Singularity-free dynamic equations of vehicle-manipulator systems," *Simulation Modelling Practice and Theory*, vol. 18, no. 6, pp. 712–731, 2010.

[8] P. Santini and P. Gasbarri, "Dynamics of multibody systems in space environment; Lagrangian vs. Eulerian approach," *Acta Astronautica*, vol. 54, no. 1, pp. 1–24, 2004.

[9] T. R. Kane and D. A. Levinson, *Dynamics, theory and applications*, McGraw–Hill Book Company, New York, 1985.

[10] C. M. Roithmayr and D. H. Hodges, "Dynamics: theory and application of Kane's method," *Journal of Computational and Nonlinear Dynamics*, vol. 11, no. 6, 2016.

[11] A. H. Bajodah, D. H. Hodges, and Y.-H. Chen, "New form of Kane's equations of motion for constrained systems," *Journal of Guidance, Control, and Dynamics*, vol. 26, no. 1, pp. 79–88, 2003.

[12] A. H. Bajodah, D. H. Hodges, and Y.-H. Chen, "Nonminimal Kane's equations of motion for multibody dynamical systems subject to nonlinear nonholonomic constraints," *Multibody System Dynamics*, vol. 14, no. 2, pp. 155–187, 2005.

[13] Y. Xu and M. Huang, "A new method of robotic dynamic analysis—Kane method," *Journal of Sichuan Institute of Light Industry and Chemical Technology*, vol. 8, no. 4, pp. 28–33, 1995.

[14] Z. Yin and X. Ge, "Dynamics analysis of a dual-arm space robot using Kane-Huston method," *Mechanical Science and Technology for Aerospace Engineering*, vol. 31, no. 8, pp. 1344–1348, 2012.

[15] F. C. Park, J. E. Bobrow, and S. R. Ploen, "A lie group formulation of robot dynamics," *The International Journal of Robotics Research*, vol. 14, no. 6, pp. 609–618, 1995.

[16] R. M. Murray, S. S. Sastry, and Z. Li, *A Mathematical Introduction to Robotic Manipulation*, CRC Press, London, 1994.

[17] F. H. Liu and H. T. Wu, "Research on modeling of robot manipulator dynamics based on screw theory," *Journal of Jiangsu University Science and Technology (Natural Science Edition)*, vol. 22, no. 2, pp. 52–55, 2008.

[18] C. Liu, J. Yuan, and M. Li, "Motion control algorithm of coordination manipulation for multi-arms free flying space robots," *Journal of Harbin Institute of Technology*, vol. 36, no. 10, pp. 1338–1340, 2004.

[19] H. Patolia, P. M. Pathak, and S. C. Jain, "Force control in single DOF dual arm cooperative space robot," in *Proceedings of the 2010 Spring Simulation Multiconference*, pp. 1–8, Orlando, Florida, 2010.

[20] M. W. Spong, "On the robust control of robot manipulators," *IEEE Transactions on Automatic Control*, vol. 37, no. 11, pp. 1782–1786, 1992.

[21] A. Zhu, H. P. Ai, and L. Chen, "A fuzzy logic reinforcement learning control with spring-damper device for space robot capturing satellite," *Applied Sciences*, vol. 12, no. 5, p. 2662, 2022.

[22] M. P. Polverini, A. M. Zanchettin, S. Castello, and P. Rocco, "Sensorless and constraint-based peg-in-hole task execution with a dual-arm robot," in *2016 IEEE International Conference on Robotics and Automation (ICRA)*, pp. 415–420, Stockholm, Sweden, 2016.

[23] H. Li and Z. Liang, "Continual motion control based on RGJM for space robot," in *2015 International Conference on Computer Science and Mechanical Automation (CSMA)*, pp. 292–296, Hangzhou, China, 2015.

[24] M. Galicki, "Finite-time trajectory tracking control in a task space of robotic manipulators," *Automatica*, vol. 67, pp. 165–170, 2016.

[25] Y. Su, C. Zheng, and P. Mercorelli, "Robust approximate fixed-time tracking control for uncertain robot manipulators," *Mechanical Systems and Signal Processing*, vol. 135, article 106379, 2020.

[26] B. Xian, M. S. deQueiroz, D. Dawson, and I. Walker, "Task-space tracking control of robot manipulators via quaternion feedback," *IEEE Transactions on Robotics and Automation*, vol. 20, no. 1, pp. 160–167, 2004.

[27] H. L. Pham, V. Perdereau, B. V. Adorno, and P. Fraisse, "Position and orientation control of robot manipulators using dual quaternion feedback," in *Proceedings of 2010 IEEE International Conference on Intelligent Robots and Systems*, Taipei, Taiwan, 2010.

[28] L. Jiang, Y. Wang, and S. Xu, "Integrated 6-DOF orbit-attitude dynamical modeling and control using geometric mechanics," *International Journal of Aerospace Engineering*, vol. 2017, Article ID 4064328, 13 pages, 2017.